Global trends in the frequency and duration of temperature extremes

Frank A. La Sorte[1] • Alison Johnston[1] • Toby R. Ault[2]

[1]Cornell Lab of Ornithology, Cornell University, Ithaca, NY 14850 USA

[2]Department of Earth and Atmospheric Sciences, Cornell University, Ithaca, NY, 14853 USA

Frank A. La Sorte

fal42@cornell.edu

Abstract

Anthropogenic climate change has affected the frequency and duration of extreme climate events, including extreme heat events (EHE) and extreme cold events (ECE). How the frequency and duration of these events have changed over time across the full annual cycle globally has not been fully explored. Here, we use detrended daily estimates of minimum and maximum temperature from the ERA5 reanalysis over a 70-year period (1950-2019) to determine when and where temperatures have significantly exceeded historical variation. During this period, Antarctica and the Arctic Ocean had high EHE frequency and duration occurring throughout the year. The Nearctic, Palearctic, IndoMalaya, Australasia, and tropical eastern Pacific had high EHE frequency and duration occurring during the boreal summer. The Arctic Ocean and the Nearctic, Palearctic, and IndoMalaya had high ECE frequency and duration occurring during the boreal summer. Positive trends in EHE frequency and duration over the 41-year period were strongest within the Northern Hemisphere and weakest within Antarctica. Positive trends in ECE frequency and duration over the 41-year period were strongest within Antarctica and the southern subtropical latitudes. Negative trends in ECE frequency and duration were strongest within the Northern Hemisphere. In sum, based on detrended temperature data from 1950 to 2019, the Northern Hemisphere has experienced a pervasive increase in EHE and decrease in ECE. These results emphasize the many near-term challenges that temperature extremes are likely to pose for life on the planet and the need to advance our understanding of the long-term implications of changing climate extreme dynamics.

Keywords cold air outbreaks, climate change, climate extremes, heat waves, temperature extremes

1 Introduction

Anthropogenic climate change is affecting the frequency and duration of extreme climate events (AghaKouchak et al. 2020; Diffenbaugh et al. 2017). These extreme events encompass a variety of phenomena including extreme heat events (EHE) (Alexander et al. 2006; Coumou and Robinson 2013; Fischer and Knutti 2015) and extreme cold events (ECE) (Walsh et al. 2001; Wheeler et al. 2011). There is evidence that exposure to EHE adversely affects human populations (Anderson and Bell Michelle 2011; Battisti and Naylor 2009; Guo et al. 2017; Mitchell et al. 2016) and natural systems within terrestrial (Harris et al. 2018; Maxwell et al. 2019) and marine environments (Garrabou et al. 2009; Wernberg et al. 2013). There is similar evidence that ECE adversely affects human populations (Smith and Sheridan 2019) and natural systems within terrestrial environments (Maxwell et al. 2019). For species in natural systems, EHE and ECE can further the decline and extirpation of populations, increasing the chances of extinction (Maron et al. 2015; Maxwell et al. 2019). EHE and ECE can also promote the formation of novel ecosystems (Harris et al. 2018), generate enhanced selection pressures (Grant et al. 2017; Gutschick and BassiriRad 2003), and change the phenology of life history events (Cremonese et al. 2017; La Sorte et al. 2016).

How the frequency and duration of EHE has changed over time has been explored primarily within terrestrial regions during the boreal and austral summers (Coumou and Robinson 2013; Oswald 2018), but there are examples that have considered other seasons of the year (Alexander et al. 2006). Within marine environments, the primary focus has been on documenting "marine heatwaves" or extreme warming in sea surface temperatures. Marine heatwaves have increased in frequency and duration across the globe (Frölicher et al. 2018; Oliver et al. 2018). These events have significantly affected the composition and structure of marine ecosystems (Smale et al. 2019). Sea surface temperature tend to be higher and less variable on average compared to the air temperature on the ocean's surface (Cayan 1980). Research examining the frequency and duration of ECE has focused primarily on cold-air outbreaks within the North Hemisphere during the boreal winter (Kolstad et al. 2010; Kretschmer et al. 2018). In total, how the frequency and duration of both EHE and ECE have changed over time across the full annual cycle within terrestrial and marine environments globally has not been fully explored.

There are a number of climate indices that have been used to estimate the occurrence of EHE (Fenner et al. 2019; Smith et al. 2013) and ECE (Smith and Sheridan 2018). These indices are often context specific and there is little consensus on the most appropriate technique (McPhillips et al. 2018). Here, we define the occurrence of EHE and ECE using a probabilistic framework that estimates the novelty of each event relative to historical year-to-year variation in temperature. We use detrended (Wu et al. 2007) daily measures of minimum and maximum temperature to estimate when and where temperatures significantly exceed historical variation over a 70-year period (1950 to 2019). The greater the deviation from historical variation, the more unusual the event and the more likely it will have adverse effects on human and natural

systems (Williams and Jackson 2007; Williams et al. 2007). This approach provides a standardized method for assessing novelty that allows for valid comparisons across space and time. We use this approach to determine how the frequency and duration of EHE and ECE have changed over time, and we identify the regions and seasons where these events are likely to have the most significant effects on natural and human populations now and into the future.

2 Materials and methods

We compiled gridded climate data from the European Centre for Medium-Range Weather Forecasts (ECMWF) fifth generation atmospheric reanalysis of the global climate (ERA5)(Hersbach et al. 2019b; Hoffmann et al. 2019). Key improvements provided by ERA5 over its predecessor includes broader data assimilation, improvements in global radiation budgets, better representation of tropospheric circulation, enhanced spatial and temporal resolutions, improved temporal consistency, and the ability to better resolve extreme events (Hersbach et al. 2019b). Reanalysis products rely on data assimilation where observations and model-based forecasts are used to generate spatially comprehensive estimates of climate variables at regular intervals over long time periods (Parker 2016). These characteristics are required when estimating global trends in the frequency and duration of temperature extremes. The chief difference between reanalysis products and related climate observations is that the errors and uncertainties associations with reanalysis products are often less well understood (Parker 2016).

For our analysis, we used the ERA5 climate variable hourly air temperature at 2 m above the surface gridded at a 31 km (0.28125° at the equator) spatial resolution over a 70-year period: 1950 to 1978 (Bell et al. 2020) and 1979 to 2019 (Hersbach et al. 2019a). We used this climate variable to first extract the minimum and maximum temperature for each day and grid cell over the 70-year period. To reduce the influence of warming trends on our analysis, we detrended the minimum and maximum temperature time series separately for each day and grid cell using the Complete Ensemble Empirical Mode Decomposition with Adaptive Noise (CEEMDAN) procedure (Torres et al. 2011). CEEMDAN is a variant of the Ensemble Empirical Mode Decomposition (EEMD) procedure (Wu and Huang 2009), which is a white noise assisted refinement of the Empirical Mode Decomposition (EMD) procedure (Huang et al. 1998; Wu et al. 2007). EMD is a highly adaptive method that is well suited to decompose non-stationary and non-linear time series. EMD has been broadly applied in climate research and is an effective method for identifying the primary characteristics of global warming (Molla et al. 2007). The EMD procedure partitions time series into intrinsic modes of oscillation (Intrinsic Mode Functions; IMFs) based on the principle of local scale separation (Huang et al. 1998; Wu et al. 2007). The IMFs are extracted level by level until no complete oscillation can be identified. EEMD consists of "sifting" an ensemble of white noise-added signal, and CEEMDAN provides an exact reconstruction of the original signal and a better spectral separation of the IMFs. The residuals that remain after the implementation of the IMF partitioning procedure defines a

monotonic time series that can be used to detrend the original data. In this case, we detrended the minimum temperature time series by subtracting the minimum temperature CEEMDAN residuals (Fig. S1) from the minimum temperature time series by day within each grid cell. Similarly, we detrended the maximum temperature time series by subtracting the maximum temperature CEEMDAN residuals (Fig. S2) from the maximum temperature time series by day within each grid cell. Factors that can limit the value of EMD detrended time series include end effects and high stochasticity (Stallone et al. 2020). The CEEMDAN variant reduces the influence of end effects (Wu and Huang 2009) and is more efficient in recovering signals from noisy data (Colominas et al. 2012).

We used the following methods to estimate the occurrence of extreme heat events (EHE) and extreme cold events (ECE) for each day within each grid cell over the 70-year period (Fig. S3). We treated the detrended minimum and maximum temperature values as normally distributed across years for each day and grid cell, an assumption that our data achieved in most cases (Fig. S4). We estimated the probability density function for minimum and maximum temperature using the mean and standard deviation calculated across years for each day and grid cell. EHE occurred when the probabilities for both minimum and maximum temperature on a given day within a given grid cell were within the 0.025 quantile of the right tail (0.975-1.00) of the two probability density functions (Fig. S3). ECE occurred when the probabilities for both minimum and maximum temperature on a given day within a given grid cell were within the 0.025 quantile of the left tail (0.00-0.025) of the two probability density functions (Fig. S3). This approach follows from previous studies where interannual climatic variation is used as a baseline to identify climatic novelty (La Sorte et al. 2018; Williams et al. 2007). Here, we used interannual variation in 70 years of detrended minimum and maximum temperature data to define our baseline, and extreme events occurred when both minimum and maximum temperature achieved unusual levels. This approach tends capture large-scale, multiday EHE and ECE events (see Appendix 1).

We summarized EHE and ECE for each year and grid cell using two measures. The first estimated the frequency of extreme events based on the proportion of days containing each event per year within each grid cell. The second estimated the duration of each event per year within each grid cell. For the first measure, we calculated the annual proportion of days within each year for each grid cell where an event occurred. To provide a spatial summary, we averaged the annual proportion of days containing each event across years for each grid cell. This approach identified grid cells that had high numbers of extreme events across all days and years. To summarize the time series, we modeled the change in the annual proportion of days for each event across years using beta regression with a logit link function and an identity function in the precision model (Ferrari and Cribari-Neto 2004; Simas et al. 2010). We removed zeros and ones using the transformation $(y \cdot (n - 1) + 0.5) / n$ where y is the vector of proportions and n is the sample size (Smithson and Verkuilen 2006). We selected beta regression because it is well suited to model continuous proportions whose values occur in the standard unit interval (0, 1). The probability density function of the beta distribution can take on a wide variety of different

shapes, providing the flexibility necessary to model continuous proportions across many settings. Thus, unlike traditional linear regression, using beta regression to model continuous proportions enhances interpretability and inferential quality (Ferrari and Cribari-Neto 2004).

Our second measure estimated the duration of each extreme event for each year and grid cell based on the number of consecutive days containing EHE or ECE. For our analysis, we extracted the maximum duration of EHE and ECE for each year and grid cell. This approach identified the longest extreme event that occurred during each year. We selected the maximum because the duration tended to be strongly right skewed and the mean did not provide a consistent estimate of central tendency. For our spatial summary, we averaged the maximum duration of each event across years for each grid cell. To summarize the time series, we modeled the change in the maximum duration in each event across years using Poisson regression (Lambert 1992). We selected Poisson because our measure of duration (number of days) is a non-negative integer that can be interpreted as a count. Using traditional linear regression with response variables that are counts will usually violate the distributional assumptions of the model and generate less robust inferences (Warton et al. 2016).

To provide a regional summary of our two measures, we examined the distribution of the regression coefficients from each measure across seven biogeographical realms (Olson and Dinerstein 2002; Pielou 1979) and seven oceans (Flanders Marine Institute 2018). The seven biogeographical realms include the Afrotropics, Antarctic, Australasia, IndoMalaya, Nearctic, Neotropics, and Palearctic. The seven oceans include the Arctic, Indian, North Atlantic, North Pacific, South Atlantic, South Pacific, and Southern Ocean. We used permutation one-way ANOVA tests with 9,999 replicates to assess if the distributions of each measure were identical across realms and oceans (Weiss 2015).

To provide a seasonal summary of EHE and ECE, we calculated the proportion of grid cells for each day and year that contained EHE and ECE within the seven biogeographical realms and seven oceans. We modeled how these proportions changed across the annual cycle for each realm and ocean using generalized additive mixed models with year included as a random effect (Wood 2017). We used a cyclic cubic regression spline to smoothly connect the beginning and end of each year. Because the response variable was a continuous proportion, we used a beta regression family with a logit link function, and we removed zeros and ones using the transformation described above.

We conducted all analysis in R, version 4.0.3 (R Development Core Team 2020). We implemented the detrending analysis using the ceemdan function in the Rlibeemd library based on the default parameters (Helske and Luukko 2018; Luukko et al. 2016). We implemented beta regression using the betareg function in the betareg library (Cribari-Neto and Zeileis 2010), and Poisson regression using the glm function in the stats library. We used the onesampb function in the WRS2 library to estimate the one-sample percentile bootstrap using 9,999 bootstrap samples (Mair and Wilcox 2019). We used the perm.oneway.anova function in the wPerm library to

implement the permutation one-way ANOVA tests (Weiss 2015). We implemented the generalized additive mixed models using the gam function in the mgcv library (Wood 2017).

3 Results

3.1 Spatial summary

The proportion of the year containing EHE and ECE presented variables patterns across the globe (Fig. 1a-b). Within terrestrial environments, the distribution of EHE proportions differed across realms (F = 2,082.8, P<0.001) with higher values occurring throughout the Antarctic, within the northern latitudes of the Nearctic and Palearctic, and within the central Afrotropics (Figs. 1a, 2a). The distribution of ECE proportions differed across realms (F = 440.2, P<0.001) with higher values occurring throughout the Antarctic, Nearctic, and Palearctic (Figs. 1b, 2b). Within marine environments, the distribution of EHE proportions differed across oceans (F = 659.8, P<0.001) with higher values occurring within the Arctic Ocean, the tropical eastern Pacific, and the tropical Atlantic (Figs. 1a, 2c). The distribution of ECE proportions differed across oceans (F = 141.6, P<0.001) with higher values occurring primarily within the mid-latitudes of both hemispheres (Figs. 1b, 2d).

The maximum duration of EHE and ECE presented contrasting patterns across the globe (Fig. 1c-d). Within terrestrial environments, the distribution of EHE duration differed across realms (F = 2,148.0, P<0.001) with higher values occurring throughout the Antarctic, the northern latitudes of the Nearctic and Palearctic, and within the central Afrotropics (Figs. 1c, 2e). The distribution of ECE duration differed across realms (F = 483.2, P<0.001) with higher values occurring within the Antarctic and the northern latitudes of the Nearctic and Palearctic (Figs. 1d, 2f). Within marine environments, the distribution of EHE duration differed across oceans (F = 850.0, P<0.001) with higher values occurring within the Arctic Ocean and the tropical eastern Pacific (Figs. 1c, 2g). The distribution of ECE duration differed across oceans (F = 271.7, P<0.001) with higher values occurring primarily within the mid-latitudes of both hemispheres (Figs. 1d, 2h).

3.2 Time series

The time series in the proportion of the year containing EHE and ECE presented variable trends across the globe (Fig. 3a-b). Within terrestrial environments, the distribution of EHE trends differed across realms (F = 358.6, P<0.001) with a greater prevalence of positive trends within the Antarctic and Australasia and a greater prevalence of negative trends within the Afrotropics (Figs. 3a, 4a). The distribution of ECE proportion trends differed across realms (F = 354.2, P<0.001) with a greater prevalence of positive trends with the Antarctic and Neotropics and a greater prevalence of negative trends with the Nearctic and Palearctic (Figs. 3b, 4b). Within

marine environments, the distribution of EHE proportion trends differed across oceans (F = 178.5, P<0.001) with positive trends occurring in greater prevalence across the world's oceans, especially the Indian Ocean, with the Arctic Ocean having the lowest prevalence (Figs. 3a, 4c). The distribution of ECE proportion trends differed across oceans (F = 237.7, P<0.001) with positive trends occurring in greater prevalence across the world's oceans, especially the Southern Ocean, with the North Atlantic having the lowest prevalence (Figs. 3b, 4d).

The time series in the maximum duration of EHE and ECE presented variable trends across the globe (Fig. 3c-d). Within terrestrial environments, the distribution of EHE duration trends differed across realms (F = 241.3, P<0.001) with a greater prevalence of positive trends within the Antarctic and Australasia and a greater prevalence of negative trends within the Afrotropics (Figs. 3c, 4e). The distribution of ECE duration trends differed across realms (F = 68.1, P<0.001) with a greater prevalence of negative trends in the Nearctic and Palearctic and a greater prevalence of positive trends in the remaining realms (Figs. 3d, 4f). Within marine environments, the distribution of EHE duration trends differed across oceans (F = 58.6, P<0.001) with a greater prevalence of positive trends occurring across all the world's oceans (Figs. 3c, 4g). The distribution of ECE duration trends differed across oceans (F = 92.1, P<0.001) with positive trends occurring in greater prevalence across the world's oceans with the North Atlantic having the lowest prevalence (Figs. 3d, 4h).

3.3 Annual cycle

When summarized by day across the annual cycle, the proportion of the 70 years containing EHE and ECE presented contrasting patterns across terrestrial environments (Fig. 5a-b). The Antarctic had the highest EHE proportion across the annual cycle with limited seasonal variation (Fig. 5a). The Nearctic and Palearctic had intermediate EHE proportions that peaked during the boreal summer (Fig. 5a). The remaining realms had the lower EHE proportions that contained limited seasonal variation (Fig. 5a). ECE proportions presented limited seasonal variation with the Antarctic, Nearctic, and Palearctic presented higher ECE proportions that peaked in December in the Nearctic and Palearctic (Fig. 5b).

When summarized by day across the annual cycle, the proportion of the 70 years containing EHE and ECE presented contrasting patterns across marine environments (Fig. 5c-d). The Arctic Ocean presented the highest EHE proportions that peaked during the boreal summer (Fig. 5c). The North Atlantic and North Pacific had intermediate EHE proportions during the boreal summer and the lowest EHE proportions during the boreal winter (Fig. 5c). The South Pacific had intermediate EHE proportions with little seasonal variation, and the remaining oceans had the lowest EHE proportions with little seasonal variation (Fig. 5c). ECE proportions presented limited differences among oceans and little seasonal variation except for the Southern Ocean whose ECE proportions peaked in March (Fig. 5d).

4 Discussion

Our assessment of 70 years of detrended temperature data identified global patterns and trends in the frequency and duration of extreme temperature events. The highest EHE frequency and duration occurred within the Antarctic and the Arctic Ocean. The Antarctic showed little seasonal variation whereas the Arctic Ocean presented a seasonal peak during the boreal summer. ECE frequency and duration, in contrast, showed greater spatial heterogeneity, with the mid-latitudes tending to have higher values and equatorial regions lower values. EHE frequency and duration was dominated by negative trends within terrestrial environments, especially in the Afrotropics, except for Antarctica and Australasia. Within marine environments, trends in EHE frequency and duration were more consistently positive. ECE frequency and duration showed a greater prevalence of positive trends within terrestrial environments, except for the Nearctic and Palearctic. Within marine environments, ECE frequency and duration presented more consistent positive trends.

A combination of atmospheric mechanisms is often associated with the occurrence of extreme temperature events. This includes mid-latitude blocking events within the Northern Hemisphere that obstruct ambient westerly winds and associated synoptic weather systems. Atmospheric blocking can generate extended periods of extreme heat (Pfahl and Wernli 2012; Röthlisberger et al. 2016) or extreme cold (Buehler et al. 2011; Sillmann et al. 2011; Whan et al. 2016). A recurrent Rossby wave pattern may act to enhance the persistence of these blocking events in the Northern Hemisphere (Röthlisberger et al. 2019). Atmospheric blocking also occurs within the mid-latitude of the Southern Hemisphere (Mendes and Cavalcanti 2014), with Northern Hemisphere blocking events tend to be stronger than those in the Southern Hemisphere (Lupo et al. 2019). Our findings suggest mid-latitude blocking are promoting ECE across the northern and southern mid-latitudes and is promoting EHE primarily at the higher latitudes within the Arctic and Antarctic.

Our findings identified the tropical eastern Pacific as a region with high EHE frequency and duration. This outcome is likely related to the air-sea interactions of the El Niño–Southern Oscillation (ENSO) whose sea-surface temperature phases can affect surface air temperatures over the tropical Pacific (Trenberth et al. 2002; Trenberth et al. 2005). The ENSO alternates irregularly between warming (El Niño) and cooling (La Niña) of sea surface temperatures in the tropical eastern Pacific. There is debate on how ENSO is being affected by climate change with evidence pointing towards an increasing frequency of extreme El Niño and La Niña events (Cai et al. 2014; Cai et al. 2015; Wang et al. 2017). Our EHE findings for the tropical eastern Pacific highlights the dominant role of ENSO in the global climate, and our findings for increasing EHE durations within this region suggest a more prominent role for ENSO in the future.

How ECE are being affected by climate change is largely absent from the literature with most studies exploring the patterns and causes of cold-air outbreaks within the mid-latitudes of the Northern Hemisphere (Kolstad et al. 2010; Kretschmer et al. 2018). In this study, we provide the first global assessment of ECE patterns and trends. Our findings emphasize that ECE

frequency and duration is declining within many terrestrial regions, primarily in the Northern Hemisphere, and is increasing across large portions of the globe, primarily within marine environments. Additional effort is needed to understand these patterns and their implications.

Our study provides the first global full annual cycle assessment using a 70-year time series of detrended temperature data of EHE and ECE patterns and trends. Our findings provide the basis to document and model the implications of changes in climate extreme dynamics for human populations (AghaKouchak et al. 2020) and the ecological and evolutionary implications for natural systems (Bailey and van de Pol 2016). Our findings emphasize the many near-term challenges that temperature extremes are likely to pose for life on the planet, most notably within the world's marine environments, and the need to advance our understanding of the long-term implications of changing climate extreme dynamics.

Acknowledgements We thank two enormous reviewers for construction comments on an earlier draft, D. Sheldon and The College of Information and Computer Sciences, University of Massachusetts for computational support.

Funding Information This research was supported by The Wolf Creek Charitable Foundation and the National Science Foundation (DBI-1939187; DEB-2017817).

References

AghaKouchak A et al. (2020) Climate extremes and compound hazards in a warming world. Annual Review of Earth and Planetary Sciences 48:519-548. doi:10.1146/annurev-earth-071719-055228

Alexander LV et al. (2006) Global observed changes in daily climate extremes of temperature and precipitation. J Geophys Res Atmos 111:D05109. doi:10.1029/2005JD006290

Anderson GB, Bell Michelle L (2011) Heat waves in the United States: Mortality risk during heat waves and effect modification by heat wave characteristics in 43 U.S. communities. Environ Health Perspect 119:210-218. doi:10.1289/ehp.1002313

Bailey LD, van de Pol M (2016) Tackling extremes: challenges for ecological and evolutionary research on extreme climatic events. J Anim Ecol 85:85-96. doi:10.1111/1365-2656.12451

Battisti DS, Naylor RL (2009) Historical warnings of future food insecurity with Uunprecedented seasonal heat. Science 323:240. doi:10.1126/science.1164363

Bell B et al. (2020) ERA5 hourly data on single levels from 1950 to 1978 (preliminary version). Copernicus Climate Change Service (C3S) Climate Data Store (CDS). (Accessed on < 12-01-2020 >), https://cds.climate.copernicus-climate.eu/cdsapp#!/dataset/reanalysis-era5-single-levels-preliminary-back-extension?tab=overview.

Buehler T, Raible CC, Stocker TF (2011) The relationship of winter season North Atlantic blocking frequencies to extreme cold or dry spells in the ERA-40. Tellus A: Dynamic Meteorology and Oceanography 63:174-187. doi:10.1111/j.1600-0870.2010.00492.x

Cai W et al. (2014) Increasing frequency of extreme El Nino events due to greenhouse warming. Nature Clim Change 4:111-116. doi:10.1038/nclimate2100
Cai W et al. (2015) ENSO and greenhouse warming. Nat Clim Chang 5:849-859. doi:10.1038/nclimate2743
Cayan DR (1980) Large-Scale relationships between sea surface temperature and surface air temperature. Mon Weather Rev 108:1293-1301. doi:10.1175/1520-0493(1980)108<1293:LSRBSS>2.0.CO;2
Colominas MA, Schlotthauer G, Torres M, Flandrin P (2012) Noise-assisted EMD methods in action. Advances in Data Science and Adaptive Analysis 4
Coumou D, Robinson A (2013) Historic and future increase in the global land area affected by monthly heat extremes. Environ Res Lett 8:034018. doi:10.1088/1748-9326/8/3/034018
Cremonese E, Filippa G, Galvagno M, Siniscalco C, Oddi L, Morra di Cella U, Migliavacca M (2017) Heat wave hinders green wave: The impact of climate extreme on the phenology of a mountain grassland. Agric For Meteorol 247:320-330. doi:10.1016/j.agrformet.2017.08.016
Cribari-Neto F, Zeileis A (2010) Beta Regression in R. Journal of Statistical Software 34:1-24.
Diffenbaugh NS et al. (2017) Quantifying the influence of global warming on unprecedented extreme climate events. Proc Natl Acad Sci U S A 114:4881. doi:10.1073/pnas.1618082114
Fenner D, Holtmann A, Krug A, Scherer D (2019) Heat waves in Berlin and Potsdam, Germany – Long-term trends and comparison of heat wave definitions from 1893 to 2017. Int J Climatol 39:2422-2437. doi:10.1002/joc.5962
Ferrari S, Cribari-Neto F (2004) Beta regression for modelling rates and proportions. Journal of Applied Statistics 31:799-815. doi:10.1080/0266476042000214501
Fischer EM, Knutti R (2015) Anthropogenic contribution to global occurrence of heavy-precipitation and high-temperature extremes. Nat Clim Chang 5:560. doi:10.1038/nclimate2617
Flanders Marine Institute (2018) IHO Sea Areas, version 3. Available online at http://www.marineregions.org/. doi:10.14284/323
Frölicher TL, Fischer EM, Gruber N (2018) Marine heatwaves under global warming. Nature 560:360-364. doi:10.1038/s41586-018-0383-9
Garrabou J et al. (2009) Mass mortality in Northwestern Mediterranean rocky benthic communities: effects of the 2003 heat wave. Glob Change Biol 15:1090-1103. doi:10.1111/j.1365-2486.2008.01823.x
Grant PR, Grant BR, Huey RB, Johnson MTJ, Knoll AH, Schmitt J (2017) Evolution caused by extreme events. Philos Trans R Soc Lond B Biol Sci 372:20160146. doi:10.1098/rstb.2016.0146
Guo Y et al. (2017) Heat wave and mortality: A multicountry, multicommunity study. Environ Health Perspect 125:087006. doi:10.1289/EHP1026
Gutschick VP, BassiriRad H (2003) Extreme events as shaping physiology, ecology, and evolution of plants: toward a unified definition and evaluation of their consequences. New Phytol 160:21-42. doi:10.1046/j.1469-8137.2003.00866.x
Harris RMB et al. (2018) Biological responses to the press and pulse of climate trends and extreme events. Nat Clim Chang 8:579-587. doi:10.1038/s41558-018-0187-9

Helske J, Luukko P (2018) Rlibeemd: Ensemble empirical mode decomposition (EEMD) and its complete variant (CEEMDAN). R package version 1.4.1. https://github.com/helske/Rlibeemd.

Hersbach H et al. (2019a) ERA5 monthly averaged data on single levels from 1979 to present. Copernicus Climate Change Service (C3S) Climate Data Store (CDS). (Accessed on < 02-14-2020 >). DOI: 10.24381/cds.f17050d7.

Hersbach H et al. (2019b) Global reanalysis: goodbye ERA-Interim, hello ERA5. ECMWF Newsletter:17-24.

Hoffmann L et al. (2019) From ERA-Interim to ERA5: the considerable impact of ECMWF's next-generation reanalysis on Lagrangian transport simulations. Atmos Chem Phys 19:3097-3124. doi:10.5194/acp-19-3097-2019

Huang NE et al. (1998) The empirical mode decomposition and the Hilbert spectrum for nonlinear and non-stationary time series analysis. P Roy Soc Lond A Mat 454:903-995. doi:10.1098/rspa.1998.0193

Kolstad EW, Breiteig T, Scaife AA (2010) The association between stratospheric weak polar vortex events and cold air outbreaks in the Northern Hemisphere. Q J R Meteorol Soc 136:886-893. doi:10.1002/qj.620

Kretschmer M, Cohen J, Matthias V, Runge J, Coumou D (2018) The different stratospheric influence on cold-extremes in Eurasia and North America. Climate and Atmospheric Science 1:44. doi:10.1038/s41612-018-0054-4

La Sorte FA, Fink D, Johnston A (2018) Seasonal associations with novel climates for North American migratory bird populations. Ecol Lett 21:845-856. doi:10.1111/ele.12951

La Sorte FA, Hochachka WM, Farnsworth A, Dhondt AA, Sheldon D (2016) The implications of mid-latitude climate extremes for North American migratory bird populations. Ecosphere 7:e01261.

Lambert D (1992) Zero-inflated Poisson regression, with an application to defects in manufacturing. Technometrics 34:1-14. doi:10.2307/1269547

Lupo AR, Jensen AD, Mokhov II, Timazhev AV, Eichler T, Efe B (2019) Changes in global blocking character in recent decades. Atmosphere 10:92.

Luukko PJ, Helske J, Räsänen E (2016) Introducing libeemd: A program package for performing the ensemble empirical mode decomposition. Comput Stat 31:545-557. doi:10.1007/s00180-015-0603-9

Mair P, Wilcox R (2019) Robust statistical methods in R using the WRS2 package. Beh Res Meth doi:10.3758/s13428-019-01246-w

Maron M, McAlpine CA, Watson JEM, Maxwell S, Barnard P (2015) Climate-induced resource bottlenecks exacerbate species vulnerability: a review. Divers Distrib 21:731-743. doi:10.1111/ddi.12339

Maxwell SL et al. (2019) Conservation implications of ecological responses to extreme weather and climate events. Divers Distrib 25:613-625. doi:10.1111/ddi.12878

McPhillips LE et al. (2018) Defining extreme events: a cross-disciplinary review. Earth's Future 6:441-455. doi:10.1002/2017EF000686

Mendes MCD, Cavalcanti IFA (2014) The relationship between the Antarctic oscillation and blocking events over the South Pacific and Atlantic Oceans. Int J Climatol 34:529-544. doi:10.1002/joc.3729

Mitchell D et al. (2016) Attributing human mortality during extreme heat waves to anthropogenic climate change. Environ Res Lett 11:074006. doi:10.1088/1748-9326/11/7/074006
Molla MKI, Sumi A, Rahman MS (2007) Analysis of temperature change under global warming impact using empirical mode decomposition. International Journal of Information Technology 3:131-139.
Oliver ECJ et al. (2018) Longer and more frequent marine heatwaves over the past century. Nat Commun 9:1324. doi:10.1038/s41467-018-03732-9
Olson DM, Dinerstein E (2002) The Global 200: Priority ecoregions for global conservation. Ann Mo Bot Gard 89:199-224.
Oswald EM (2018) An analysis of the prevalence of heat waves in the United States between 1948 and 2015. J Appl Meteorol Clim 57:1535-1549. doi:10.1175/JAMC-D-17-0274.1
Parker WS (2016) Reanalyses and observations: what's the difference? B Am Meteorol Soc 97:1565-1572. doi:10.1175/bams-d-14-00226.1
Pfahl S, Wernli H (2012) Quantifying the relevance of atmospheric blocking for co-located temperature extremes in the Northern Hemisphere on (sub-)daily time scales. Geophys Res Lett 39 doi:10.1029/2012GL052261
Pielou EC (1979) Biogeography. Wiley, NY.
R Development Core Team (2020) R: A language and environment for statistical computing. R Foundation for Statistical Computing https://www.R-project.org/, Vienna, Austria.
Röthlisberger M, Frossard L, Bosart LF, Keyser D, Martius O (2019) Recurrent synoptic-scale Rossby wave patterns and their effect on the persistence of cold and hot spells. J Clim 32:3207-3226. doi:10.1175/JCLI-D-18-0664.1
Röthlisberger M, Pfahl S, Martius O (2016) Regional-scale jet waviness modulates the occurrence of midlatitude weather extremes. Geophys Res Lett 43:10,989-910,997. doi:10.1002/2016GL070944
Sillmann J, Croci-Maspoli M, Kallache M, Katz RW (2011) Extreme cold winter temperatures in Europe under the influence of North Atlantic atmospheric blocking. J Clim 24:5899-5913. doi:10.1175/2011JCLI4075.1
Simas AB, Barreto-Souza W, Rocha AV (2010) Improved estimators for a general class of beta regression models. Computational Statistics & Data Analysis 54:348-366. doi:10.1016/j.csda.2009.08.017
Smale DA et al. (2019) Marine heatwaves threaten global biodiversity and the provision of ecosystem services. Nat Clim Chang 9:306-312. doi:10.1038/s41558-019-0412-1
Smith ET, Sheridan SC (2018) The characteristics of extreme cold events and cold air outbreaks in the eastern United States. Int J Climatol 38:e807-e820. doi:10.1002/joc.5408
Smith ET, Sheridan SC (2019) The influence of extreme cold events on mortality in the United States. Sci Total Environ 647:342-351. doi:10.1016/j.scitotenv.2018.07.466
Smith TT, Zaitchik BF, Gohlke JM (2013) Heat waves in the United States: definitions, patterns and trends. Clim Change 118:811-825. doi:10.1007/s10584-012-0659-2
Smithson M, Verkuilen J (2006) A better lemon squeezer? Maximum-likelihood regression with beta-distributed dependent variables. Psychol Methods 11:54-71. doi:10.1037/1082-989X.11.1.54
Stallone A, Cicone A, Materassi M (2020) New insights and best practices for the successful use of Empirical Mode Decomposition, Iterative Filtering and derived algorithms. Sci Rep 10:15161. doi:10.1038/s41598-020-72193-2

Torres ME, Colominas MA, Schlotthauer G, Flandrin P A complete ensemble empirical mode decomposition with adaptive noise. In: 2011 IEEE International Conference on Acoustics, Speech and Signal Processing (ICASSP), 2011. pp 4144-4147. doi:10.1109/ICASSP.2011.5947265

Trenberth KE, Caron JM, Stepaniak DP, Worley S (2002) Evolution of El Niño–Southern Oscillation and global atmospheric surface temperatures. J Geophys Res Atmos 107:AAC 5-1-AAC 5-17. doi:10.1029/2000JD000298

Trenberth KE, Stepaniak DP, Smith L (2005) Interannual variability of patterns of atmospheric mass distribution. J Clim 18:2812-2825. doi:10.1175/jcli3333.1

Walsh JE, Phillips AS, Portis DH, Chapman WL (2001) Extreme cold outbreaks in the United States and Europe, 1948–99. J Clim 14:2642-2658. doi:10.1175/1520-0442(2001)014<2642:ECOITU>2.0.CO;2

Wang G et al. (2017) Continued increase of extreme El Niño frequency long after 1.5 °C warming stabilization. Nat Clim Chang 7:568-572. doi:10.1038/nclimate3351

Warton DI, Lyons M, Stoklosa J, Ives AR (2016) Three points to consider when choosing a LM or GLM test for count data. Methods Ecol Evol 7:882-890. doi:https://doi.org/10.1111/2041-210X.12552

Weiss NA (2015) wPerm: Permutation Tests. R package version 1.0.1. https://CRAN.R-project.org/package=wPerm.

Wernberg T et al. (2013) An extreme climatic event alters marine ecosystem structure in a global biodiversity hotspot. Nat Clim Chang 3:78-82. doi:10.1038/nclimate1627

Whan K, Zwiers F, Sillmann J (2016) The influence of atmospheric blocking on extreme winter minimum temperatures in North America. J Clim 29:4361-4381. doi:10.1175/JCLI-D-15-0493.1

Wheeler DD, Harvey VL, Atkinson DE, Collins RL, Mills MJ (2011) A climatology of cold air outbreaks over North America: WACCM and ERA-40 comparison and analysis. J Geophys Res Atmos 116 doi:10.1029/2011JD015711

Williams JW, Jackson ST (2007) Novel climates, no-analog communities, and ecological surprises. Front Ecol Environ 5:475-482.

Williams JW, Jackson ST, Kutzbach JE (2007) Projected distributions of novel and disappearing climates by 2100 AD. Proc Natl Acad Sci U S A 104:5738-5742.

Wood SN (2017) Generalized Additive Models: An Introduction With R. 2nd edn. Chapman & Hall/CRC, Boca Raton, FL.

Wu Z, Huang NE (2009) Ensemble empirical mode decomposition: a noise-assisted data analysis method. Advances in Adaptive Data Analysis 01:1-41. doi:10.1142/s1793536909000047

Wu Z, Huang NE, Long SR, Peng C-K (2007) On the trend, detrending, and variability of nonlinear and nonstationary time series. Proc Natl Acad Sci U S A 104:14889. doi:10.1073/pnas.0701020104

Fig. 1 The average proportion of the year containing (a) extreme heat events and (b) extreme cold events summarized over a 70-year period (1950-2019). The average maximum duration (days) of (c) extreme heat events and (d) extreme cold events summarized over a 70-year period (1950-2019).

Fig. 2 The median proportion of the year (±2 median absolute deviations) containing extreme heat events and extreme cold events within (a-b) seven biogeographical realms and (c-d) seven oceans summarized over a 70-year period (1950-2019). The median maximum duration (±2 median absolute deviations) of extreme heat events and extreme cold events within (e-f) seven biogeographical realms and (g-h) seven oceans summarized over a 70-year period (1950-2019). The seven biogeographical realms include the Afrotropics, Antarctic, Australasia, IndoMalaya, Nearctic, Neotropics, and Palearctic. The seven oceans include the Arctic, Indian, North Atlantic, North Pacific, South Atlantic, South Pacific, and Southern Ocean.

Fig. 3 The change in the proportion of the year containing (a) extreme heat events and (b) extreme cold events over a 70-year period (1950-2019). The change in the maximum duration of (c) extreme heat events and (d) extreme cold events over a 70-year period (1950-2019). Change in proportion of extreme events estimated using beta regression (units are the annual ratio of the proportion of extreme events observed to the proportion of extreme events not observed). Change in the maximum duration of extreme events estimated using Poisson regression.

Fig. 4 The median change in the proportion of the year (±2 median absolute deviations) containing extreme heat events and extreme cold events within (a-b) seven biogeographical realms and (c-d) seven oceans over a 70-year period (1950-2019). The median change in the maximum duration (±2 median absolute deviations) of extreme heat events and extreme cold events within (e-f) seven biogeographical realms and (g-h) seven oceans over a 70-year period (1950-2019) The seven biogeographical realms include the Afrotropics, Antarctic, Australasia, IndoMalaya, Nearctic, Neotropics, and Palearctic. The seven oceans include the Arctic, Indian, North Atlantic, North Pacific, South Atlantic, South Pacific, and Southern Ocean.

Fig. 5 The proportion of (a) seven biogeographical realms and (b) seven oceans containing extreme heat events by day summarized over a 70-year period (1950-2019). The proportion of (c) seven biogeographical realms and (d) seven oceans containing extreme cold events by day summarized over a 70-year period (1950-2019). The fitted lines are generalized additive mixed models using a cyclic cubic regression spline with year included as a random effect.

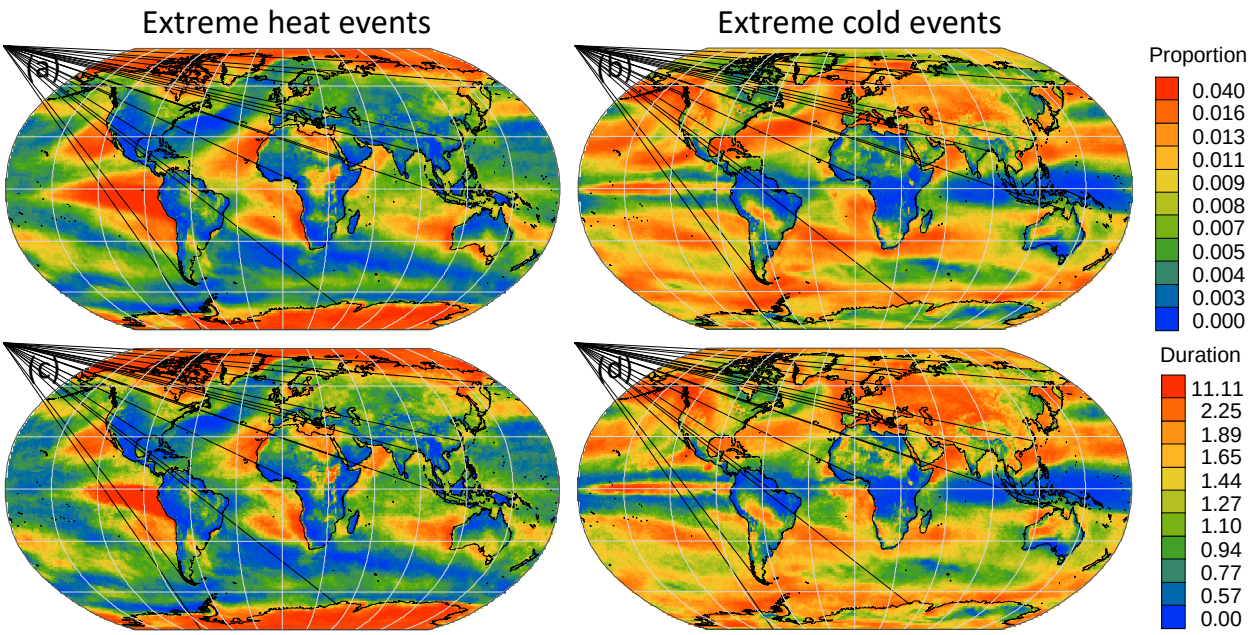
Extreme heat events
Extreme cold events
(a)
(b)
(c)
(d)
Proportion
0.040
0.016
0.013
0.011
0.009
0.008
0.007
0.005
0.004
0.003
0.000
Duration
11.11
2.25
1.89
1.65
1.44
1.27
1.10
0.94
0.77
0.57
0.00

Figure 1

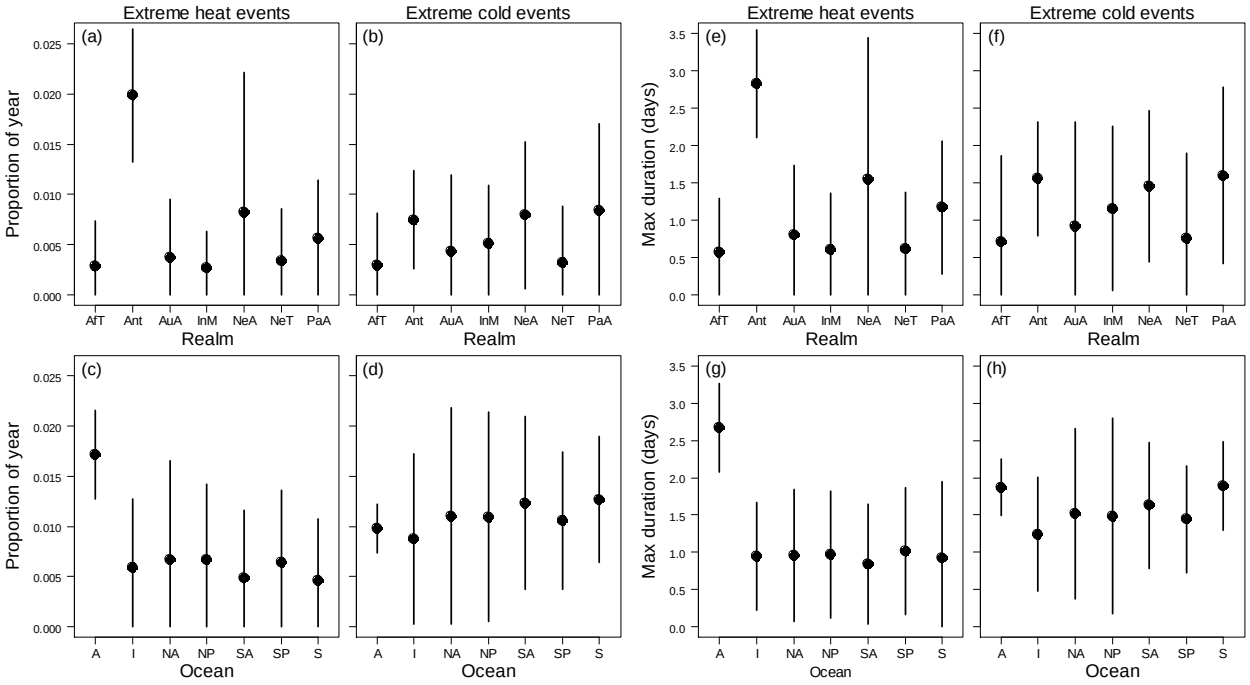
Extreme heat events
Extreme cold events
Extreme heat events
Extreme cold events
(a)
(b)
(e)
(f)
(c)
(d)
(g)
(h)
Proportion of year
Max duration (days)
Realm
Ocean
AfT
Ant
AuA
InM
NeA
NeT
PaA
A
I
NA
NP
SA
SP
S

Figure 2

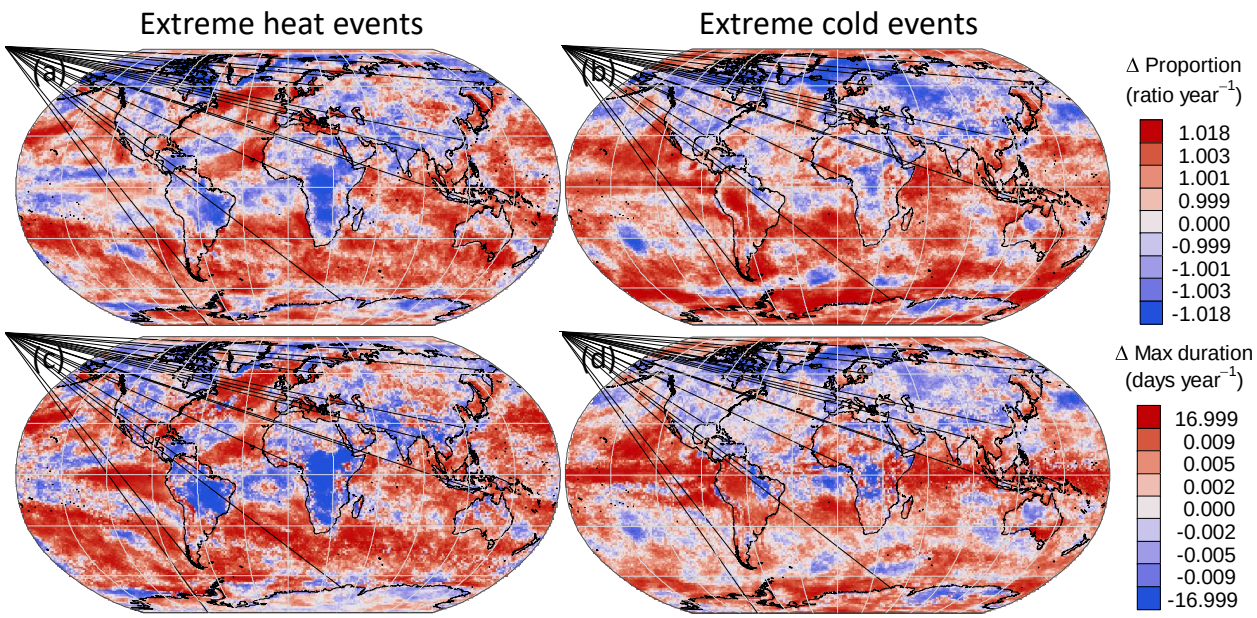
Extreme heat events
Extreme cold events
(a)
(b)
(c)
(d)
Δ Proportion
(ratio year^{-1})
1.018
1.003
1.001
0.999
0.000
-0.999
-1.001
-1.003
-1.018
Δ Max duration
(days year^{-1})
16.999
0.009
0.005
0.002
0.000
-0.002
-0.005
-0.009
-16.999

Figure 3

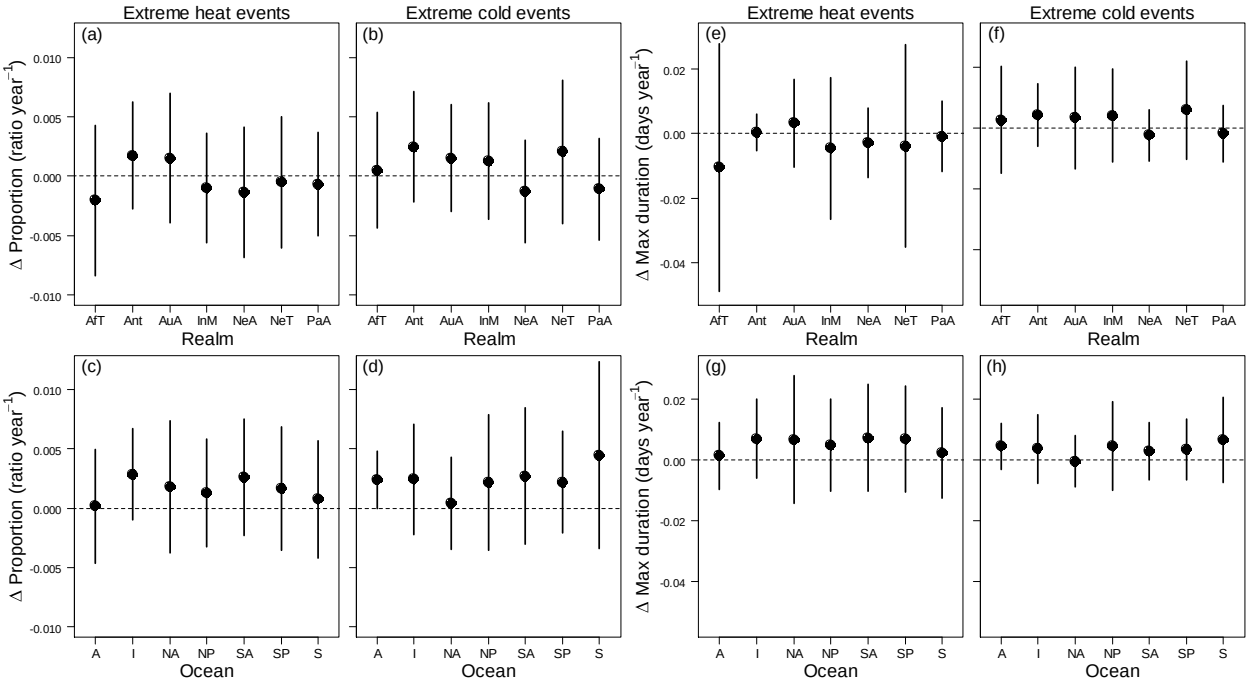
Extreme heat events
Extreme cold events
Extreme heat events
Extreme cold events
(a)
(b)
(e)
(f)
(c)
(d)
(g)
(h)
Δ Proportion (ratio year^{-1})
Δ Max duration (days year^{-1})
0.010
0.005
0.000
-0.005
-0.010
0.02
0.00
-0.02
-0.04
AfT Ant AuA InM NeA NeT PaA
Realm
A I NA NP SA SP S
Ocean

Figure 4

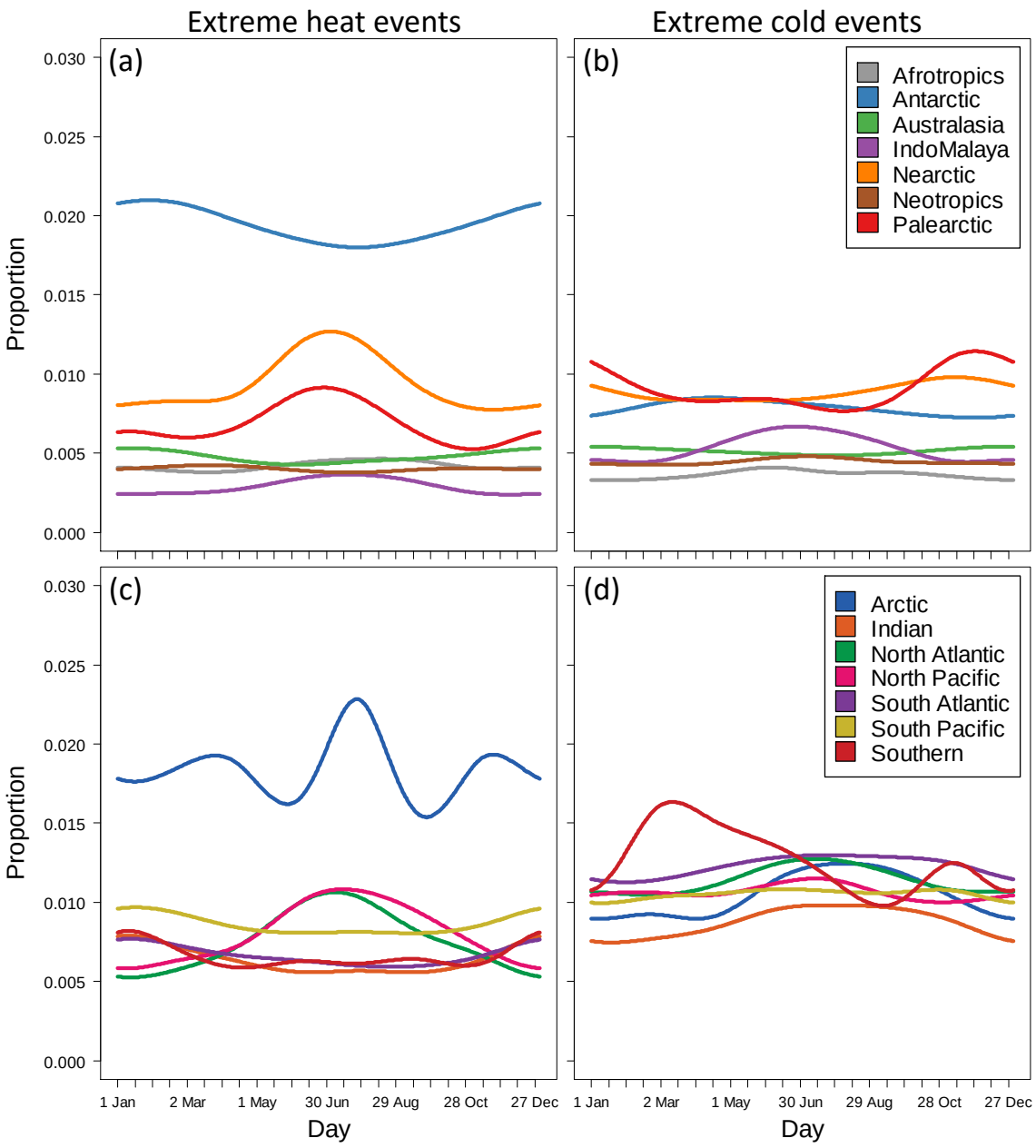
Extreme heat events
Extreme cold events
(a)
(b)
(c)
(d)
Proportion
Day
0.030
0.025
0.020
0.015
0.010
0.005
0.000
1 Jan
2 Mar
1 May
30 Jun
29 Aug
28 Oct
27 Dec
Afrotropics
Antarctic
Australasia
IndoMalaya
Nearctic
Neotropics
Palearctic
Arctic
Indian
North Atlantic
North Pacific
South Atlantic
South Pacific
Southern

Figure 5